IEEE Open Journal of the Communications Society

Received 29 July 2024; revised 2 September 2024; accepted 9 September 2024. Date of publication 13 September 2024; date of current version 8 October 2024.

Digital Object Identifier 10.1109/OJCOMS.2024.3460055

Effect of Channel Aging on Beyond Diagonal Reconfigurable Intelligent Surfaces

ANASTASIOS PAPAZAFEIROPOULOS [1,2] (Senior Member, IEEE), PANDELIS KOURTESSIS [1], AND SYMEON CHATZINOTAS [2] (Fellow, IEEE)

[1]Communications and Intelligent Systems Research Group, University of Hertfordshire, AL10 9AB Hatfield, U.K.

[2]SnT, University of Luxembourg, 1855 Luxembourg City, Luxembourg

CORRESPONDING AUTHOR: A. PAPAZAFEIROPOULOS (e-mail: tapapazaf@gmail.com)

This work was supported in part by the University of Hertfordshire's 5-Year Vice Chancellor's Research Fellowship, and in part by the National Research Fund, Luxembourg, through the Project RISOTTI.

ABSTRACT Reconfigurable intelligent surface (RIS) has appeared as a revolutionary candidate technology for future sixth-generation (6G) networks, but most works have relied on single-connected reflective RISs, which are mathematically described by diagonal phase shift matrices. In this work, based on the recently presented research on beyond diagonal (BD) RIS unifying different RIS models and architectures towards enhanced advantages such as a greater coverage, we study the impact of channel aging due to user equipment (UE) movement. Especially, we evaluate how channel aging diminishes the system performance of multiple sector BD-RIS systems. Through a robust design, concerning the average sum-rate maximisation problem, we jointly design the BD-matrix and transmit precoder under the channel aging conditions. Numerical results show how channel aging affects performance with respect to fundamental system parameters and shed light on how general aging can be compensated.

INDEX TERMS Channel aging, beyond diagonal reconfigurable intelligent surfaces, 6G networks.

I. INTRODUCTION

RECONFIGURABLE intelligent surfaces (RISs) are a revolutionary technology for wireless communications that can shape the propagation environment in a cost-efficient manner by alleviating blockage effects [1], [2], [3], [4]. An RIS consists of a two-dimensional planar software-defined surface implemented by many nearly passive elements with very low power consumption, which can change the phase shifts and the amplitudes of the incident signals. For example, in [2], authors minimized the base station (BS) transmit power under signal-to-interference-plus-noise ratio (SINR) limitations in a multi-user (MU) multiple-input single-output (MISO) communication RIS assisted communication system by jointly optimising the precoder and the passive beamforming matrix. Also, the maximisation of the sum-rate under transmit power constraints took place in [3].

RIS realisations can be met in various tunable surface designs. On one hand, the operation of an RIS can take place in three ways, which are reflection, transmission, and hybrid reflection and transmission [5], [6]. In the case of transmissive or reflective RIS, impinging signals are transmitted or reflected through or from the RIS to the opposite or the same side of the transmitter. In the case of the hybrid reflection and transmission, known as simultaneously transmitting and reflecting RIS (STAR-RIS), incident signals can be transmitted simultaneously at the two sides of the RIS. On the other hand, the scattering parameter network analysis [7] has enabled the classification of RIS into three different architectures with respect to the circuit topology among different elements. Specifically, we meet fully-, group-, and single-connected architectures. Existing literature has mostly considered the single-connected layout with each element not connected with each other [1], [2], [3], [4]. However, if some or all RIS elements become connected with each other, the RIS performance can be enhanced.

On this ground, the single-connected architecture, considered in most previous research and denoted as conventional RIS is described mathematically by a diagonal phase shift matrix. Recently, models based on beyond diagonal phase

shift matrices, namely beyond diagonal RIS (BD-RIS) have been proposed [7], [8], [9], [10], [11], [12], [13], [14]. In [7], modelling of the RIS in terms of the scattering parameter network took place. Therein, the categorization into single-, group-, and fully-connected architectures was presented. Notably, the group- and fully-connected RISs are not described by a diagonal matrix as the single RIS, which allows to optimise of not only the phase shifts but also the amplitudes of the impinging waves. Hence, the performance of RIS can be improved. This study was followed by optimal group/fully-connected design in [10], and discrete-value group/fully-connected architectures in [11]. In [8], another RIS architecture with non-diagonal phase shift matrices was proposed that provides a higher rate compared to a conventional RIS. Intelligent omnisurface (IOS)/ STAR-RIS architectures have been introduced to improve coverage [5], [6], [15]. Notably, IOS/ STAR-RIS has been proven to be a particular design of group-connected architectures with a size of group 2. In this direction, multiple sector BD-RIS has been proposed not only to improve the performance but also to provide 360° coverage.[1] In [16], a combination of multiple sector BD-RIS with rate-splitting multiple access (RSMA) was presented to improve the performance and coverage.

To reap the benefits of RIS, the acquirement of precise channel state information (CSI) is of crucial significance [17], [18], [19]. Unfortunately, channel estimation is quite challenging in RIS-assisted systems because RIS elements cannot transmit or receive any pilots which makes traditional channel estimation infeasible. Also, RIS generally consists of a large number of elements that demand prohibitively high training overhead. For example, in [17], an ON/OFF channel estimation design was suggested. Therein, the channels of a RIS-assisted MU-MISO system with just one user equipment (UE) were computed one by one. Furthermore, many works, e.g., [18], [19] do not yield analytical expressions. In [4], an effective method was proposed that has low overhead since it provides the channel estimation of the BS-RIS-UE channel in a single stage according to the minimum mean square error (MMSE) estimation method.

In this direction, it is worthwhile to mention that CSI apart from being imperfect can also become outdated in practical conditions. This phenomenon is also known as channel aging [20], [21], [22], [23], [24], [25]. In particular, in opposition to the traditional block fading model, the channel changes due to user mobility, i.e., it changes from symbol to symbol. As a result, a mismatch is observed between the estimated channel and the current channel. Generally, various works have focused on the effect of channel aging under different system architectures [20], [21], [22], [23], [25]. Especially, in [24], [25], the degradation of RIS-assisted systems due to channel aging was investigated, but its study in multiple sector BD-RIS assisted systems has not been considered yet. In [24], the authors focused on millimeter-wave (mmWave) communications with line-of-sight (LoS) links. In [25], massive multiple-input-multiple-output (MIMO) including correlated fading was studied.

A. MOTIVATION-CONTRIBUTION

Under these conditions, the motivation of this work is to characterise the effect of channel variation (aging) on the sum spectral efficiency (SE) of a multiple sector BD-RIS-assisted MU-MISO architecture, which accounts for both imperfect CSI and channel aging. Notably, the proposed model can offer substantial benefits in high-mobility environments such as dense urban areas, e.g., cellular networks with users moving at high speeds, such as in cars, trains, or airplanes. Other scenarios include: i) Millimeter-Wave (mmWave) Communication, especially in urban environments with many obstructions like buildings and vehicles. The mmWave frequencies are highly susceptible to blockage and reflection, leading to fast-varying channel conditions. Channel aging can significantly affect beamforming and beam-tracking algorithms, resulting in frequent re-alignment needs and loss of connection stability. ii) Massive MIMO systems. Specifically, channel aging can impact the accuracy of precoding and decoding processes that rely on timely and accurate CSI. In scenarios with high user mobility or rapidly changing environments, the performance of the massive MIMO system can degrade due to outdated CSI, leading to inter-user interference and suboptimal resource allocation. iii) Unmanned aerial vehicle (UAV) communications. In this case, channel aging affects the link reliability between the UAVs and their control stations due to frequent changes in altitude, orientation, and relative movement, leading to outdated CSI and hence compromised link quality.

- Contrary to existing works on BD-RIS assisted systems [7], [8], [9], [10], [11], [12], which assumed only static user equipments (UEs), we take into account user mobility in terms of channel aging.
- We achieve the maximisation of the average sum SE for multiple sector BD-RIS impaired by channel aging by proposing the robust beamforming design algorithm in [16].[2] The corresponding stochastic optimisation problem is solved through each approximation as a deterministic optimization by using the sample average approximation (SAA) [26]. Next, we result in a more tractable 3-block optimisation by using

[1]STAR-RIS is generalized in [9], which unifies different BD-RIS modes (reflective/transmissive/hybrid) and different BD-RIS architectures (single-/group-/fully-connected). In particular, a A STAR-RIS can be implemented by a BD-RIS when each of two antennas with uni-directional radiation pattern are back to back placed to form one cell, and are connected to a 2-port fully-connected reconfigurable impedance network. Also, the multiple sector BD-RIS, used in this work, has important gains over STAR-RIS due to the highly directional beam of each sector [16].

[2]Differently to [16], our optimization problem and algorithm account for channel aging. In fact, the key difference between this work and [14] is the dependency of q (the channel use), which appears on the channel and the various expressions and allows to study the impact of channel aging. Also, a summation of the channel uses appears on the derivation of the achievable rate, which affects the formulation of the optimization problem.

the weighted minimum mean square error (WMMSE)-rate method [27]. In particular, the optimization of the BD-RIS is solved by manifold methods [28].[3] Notably, we elaborate on the complexity analysis and the convergence analysis of the proposed design.

- We present simulation results that elaborate on the performance of the ergodic sum rate of multiple sector BD-RIS aided MU-MISO with respect to the mobility conditions, the quality of service threshold, and the pattern of radiation of the BD-RIS. For example, it is shown how the mobility degrades the performance while varying the number of base station antennas and the BD-RIS antennas.

B. PAPER OUTLINE

The organization of this paper is as follows. In Section II, we describe the system model of a BD-RIS-aided MU-MISO system with imperfect CSI and channel aging conditions. Section III provides the sum SE optimization. The discussion of numerical results takes place in Section IV, and the Conclusion of the paper is presented in Section V.

C. NOTATION

The symbols $(\cdot)^{\mathsf{T}}$, $(\cdot)^{\mathsf{H}}$, and $\mathrm{tr}(\cdot)$ correspond to the transpose, Hermitian transpose, and trace operators, respectively. We denote vectors and matrices by boldface lower and upper case symbols, respectively. The expectation is symbolized by $\mathbb{E}\{\cdot\}$. Moreover, $\mathrm{diag}(\mathbf{a})$ denotes a diagonal matrix with $\mathbf{a}$ being in the diagonal. Also, $\mathbf{b} \sim \mathcal{CN}(\mathbf{0}, \Sigma)$ describes a circularly symmetric complex Gaussian vector with zero mean and covariance matrix Σ.

II. SYSTEM MODEL

We rely on a BD-RIS-aided downlink MU-MISO architecture. The BS, acting as the transmitter, is deployed with M antennas, and serves a set of $\mathcal{K} = \{1, \ldots, K\}$ single-antenna UEs that are located behind obstacles, where K is the total number of served UEs. An L-cell multiple sector BD-RIS aids the communication by means of an ideal controller, which is linked to the BS, as depicted in Fig. (1).

A. MULTIPLE SECTOR BD-RIS

Herein, we describe the multiple sector BD-RIS architecture [12]. Specifically, it is modelled as a polygon that consists of in terms of L sectors. Each sector includes N antennas. The design relies on antenna arrangements and a group-connected reconfigurable impedance network. On this ground, the multiple sector BD-RIS includes N cells defining the set $\mathcal{N} = \{1, \ldots, n\}$, where cell n, $\forall n \in \mathcal{N}$ includes antennas $n, N+n, \ldots, (L-1)N+n$. The connection of these antennas is enabled by reconfigurable impedance components. The radiation pattern of each multiple sector BD-RIS antenna is uni-directional with beamwidth $2\pi/L$ that covers $1/L$ of the azimuth space. By increasing L, we achieve to narrow the beamwidth of each BD-RIS antenna, which means that the antenna gain of each BD-RIS antenna increases.

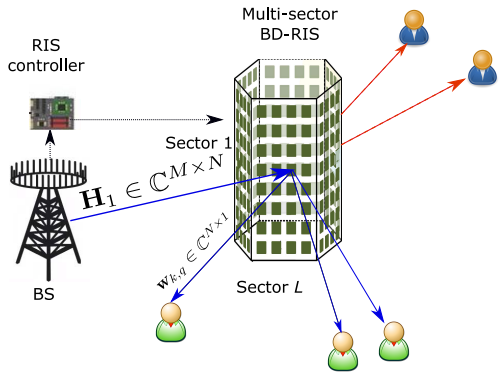

FIGURE 1. A multiple sector BD-RIS-assisted MU-MISO system.

From the mathematical point of view, the multiple sector BD-RIS is described by L matrices $\mathbf{\Phi}_l \in \mathbb{C}^{N \times N}, \forall l \in \mathcal{L} = \{1, \ldots, L\}$. The lth matrix corresponds to the lth sector, while the matrices satisfy the combined unitary constraint given by [9]

$$\sum_{l} \mathbf{\Phi}_l^{\mathsf{H}} \mathbf{\Phi}_l = \mathbf{I}_N, \tag{1}$$

which corresponds to a lossless reconfigurable impedance network. Notably, in this study, we account for the cell-wise single-connected (CW-SC) architecture of the multiple sector BD-RIS. According to this architecture, the inner-cell antennas are connected to each other by reconfigurable impedance components while the inter-cell antennas are not connected to each other. In the case of multiple sector BD-RIS with CW-SC architecture, we have that $\mathbf{\Phi}_l, \forall l \in \mathcal{L}$ are all diagonal matrices, and constraint (1) becomes

$$\mathbf{\Phi}_l = \mathrm{diag}(\phi_{l,1}, \ldots, \phi_{l,N}), \forall l, \tag{2}$$

$$\sum_{l} |\phi_{l,n}|^2 = 1, \forall n, \tag{3}$$

where $\phi_{l,n} \in \mathbb{C}, \forall l \in \mathcal{L}, \forall n \in \mathcal{N}$.

For the sake of demonstration, we consider that the BS is in sector 1, and $\mathcal{K}_l = \{\sum_{i=1}^{l-1} K_i + 1, \sum_{i=1}^{l-1} K_i + 2, \ldots, \sum_{i=1}^{l} K_i\}$ UEs are found in sector $l, \forall l \in \mathcal{L}$ with $\cup_l \mathcal{K}_l = \mathcal{K}$.

B. CHANNEL AGING

The mobility of the UEs causes a phenomenon, known as channel aging [20], [21], [22]. Specifically, a Doppler shift appears due to this movement that makes the channel change with time.[4] Thus, the channel coefficients vary

[3] Although the WMMSE method and the Riemannian manifold method are two tools that are usually used during optimization problems, we have applied suitable modifications to allow them to formulate and solve the optimization problem under channel aging conditions.

[4] Reasonably, we assume that all elements of the surface move with the same relative velocity compared to a specified UE.

among symbols, but they are invariable during the duration of one symbol. Also, we assume that the duration of the symbol duration is less than the coherence time of all UEs [20], [21], [22], [23]. The channel use is denoted by $q \in \{1, \ldots, \tau_c\}$ with τ_c channel uses.

During the qth time slot of each coherence block, let $\mathbf{H}_1 = [\mathbf{h}_{11} \ldots, \mathbf{h}_{1N}] \in \mathbb{C}^{M\times N}$ and $\mathbf{w}_{k,q} \in \mathbb{C}^{N\times 1}$ denote the LoS channel between the BS and the surface (BD-RIS) and the channel between the surface and UE k at the qth slot. We assume only LoS communication between the BS and the BD-RIS because the latter is expected to be deployed near the BS to provide better performance as in [29]. Also, we would like to mention that we ignore the direct channel connecting the BS and the UEs. However, the extension of the following study is still feasible under the presence of direct links.

The LoS channel $\mathbf{H}_1$ is assumed of full rank, and is given by [4], [30]

$$[\mathbf{H}_1]_{m,l} = \sqrt{\beta_1}\exp\Bigg(j\frac{2\pi}{\lambda}\big((m-1)d_{\mathrm{BS}}\sin\theta_{1,l}\sin\phi_{1,l} + (l-1)d_{\mathrm{RIS}}\sin\theta_{2,m}\sin\phi_{2,m}\big)\Bigg), \tag{4}$$

where β_1 denotes the path-loss of the BS-BD-RIS link, λ denotes the wavelength of the carrier, while d_{BS} and d_{RIS} denote the separation between different antennas at the BS and the separation at the RIS between different elements, respectively [31]. Also, $\phi_{1,l}$ and $\theta_{1,l}$ are the azimuth and elevation angles of departure (AoD) at the BS with respect to RIS element l, and $\phi_{2,l}$ and $\theta_{2,l}$ correspond to the azimuth and elevation LoS angles of arrival (AoA) at the RIS. The corresponding angles ϕ and θ are generated uniformly between 0 to π and 0 to 2π, respectively. Note that to benefit from the RIS in a multi-user setting, the rank of $\mathbf{H}_1$ must be greater than K.

Regarding $\mathbf{w}_{k,q}$, it is described as

$$\mathbf{w}_{k,q} = \sqrt{\beta_{\mathrm{g},k}}\mathbf{z}_{k,q}, \tag{5}$$

where $\beta_{\mathrm{g},k}$ describes the path-loss between the BD-RIS and UE k. Furthermore, $\mathbf{z}_{k,q} \sim \mathcal{CN}(\mathbf{0}, \mathbf{I}_N)$ is the fast-fading vector at the qth time slot. It is worthwhile to mention that the fast-fading vectors vary during each coherence block. Note that the path losses are considered that do not change during a large number of coherence blocks. Thus, the path losses do not depend on q but vary at every several coherence intervals. In other words, they change with time, but slower than the coherence time.

The overall channel vector is $\mathbf{H}_1\mathbf{\Phi}_l\mathbf{w}_{k,q} = \mathbf{H}_1\mathrm{diag}(\mathbf{w}_{k,q})\boldsymbol{\phi}_l$, where $\boldsymbol{\phi}_l = [\phi_{l,1}, \ldots, \phi_{l,N}]^{\mathsf{T}} \in \mathbb{C}^N, \forall l \in \mathcal{L}$. We denote $\mathbf{H}_{k,q} = \mathbf{H}_1\mathrm{diag}(\mathbf{w}_{k,q}), \forall k \in \mathcal{K}$ the overall cascaded channel between the BS and UE k.

To model channel aging, the channel realization $\mathbf{H}_{k,q}$ at the qth time instant is described in terms of its initial realization $\mathbf{H}_{k,0}$ and an innovation realization as [23]

$$\mathbf{H}_{k,q} = \delta_{k,q}\mathbf{H}_{k,0} + \bar{\delta}_{k,q}\mathbf{E}_{k,q}, \tag{6}$$

where $\mathbf{E}_{k,q}$ expresses the innovation realization at the qth time slot, and $\delta_{k,q} = \mathrm{J}_0(2\pi f_{\mathrm{D}} T_s q)$ denotes the temporal correlation coefficient of UE k between the channel realizations at time 0 and q. Note that $\mathrm{J}_0(\cdot)$ denotes the zeroth-order Bessel function of the first kind. Also, T_s is the channel sampling duration, and $f_D = \frac{vf_c}{c}$ is the maximum Doppler shift. Moreover, we have that $\bar{\delta}_{k,q} = \sqrt{1-\delta_{k,q}^2}$. Furthermore, v is the UE velocity, $c = 3\times 10^8$ m/s is the speed of light, and f_c is the carrier frequency. We observe that $\delta_{k,q}$, given in terms of the Bessel function, decreases with some ripples by increasing the velocity or the delay.

C. IMPERFECT CSI WITH CHANNEL AGING

Given that the BD-RIS is passive, the acquisition of CSI is challenging. Under practical conditions, we assume that the BS can acquire imperfect CSI $\hat{\mathbf{H}}_q = [\hat{\mathbf{H}}_{1,q}, \ldots, \hat{\mathbf{H}}_{K,q}] \in \mathbb{C}^{M\times NK}$. Specifically, we have

$$\mathbf{H}_q = \hat{\mathbf{H}}_q + \tilde{\mathbf{H}}_q, \tag{7}$$

where $\mathbf{H}_q = [\mathbf{H}_{1,q}, \ldots, \mathbf{H}_{K,q}] \in \mathbb{C}^{M\times NK}$ is the perfect cascaded channel matrix, and $\tilde{\mathbf{H}}_q = [\tilde{\mathbf{H}}_{1,q}, \ldots, \tilde{\mathbf{H}}_{K,q}] \in \mathbb{C}^{M\times NK}$ is the estimation error matrix. In this work, we assume that imperfect CSI comes from uplink training under the time division duplex (TDD) protocol according to the standard MMSE estimation [32]. Under this scenario, the channel estimation error is described by a complex Gaussian distribution, i.e., the elements of $\tilde{\mathbf{H}}_q$ follow a complex Gaussian distribution with variance r_k^2 that quantifies the imperfect CSI between the BS and UE k. The training phase takes place for $n \leq K$. Next, at the transmission phase, i.e., at $q = K+1$, the channel estimate will worsen with increasing time after the training. Taking into account (6) and (7), channel aging can by described as

$$\mathbf{H}_{k,q} = \delta_{k,q}\hat{\mathbf{H}}_{k,0} + \hat{\mathbf{E}}_{k,q}, \tag{8}$$

where $\hat{\mathbf{E}}_{k,q} = \delta_{k,q}\tilde{\mathbf{H}}_{k,0} + \bar{\delta}_{k,q}\mathbf{E}_{k,q}$.

D. DOWNLINK TRANSMISSION

During the downlink transmission, the BS broadcasts data to all UEs with the help of a precoding vector $\mathbf{f}_{k,q} \in \mathbb{C}^{M\times 1}$. During the data transmission phase ($q = K+1, \ldots, \tau_c$), the received signal $y_{k,q} \in \mathbb{C}$ by UE k can be expressed as

$$y_{k,q} = \mathbf{w}_{k,q}^{\mathsf{H}}\mathbf{\Phi}_l^{\mathsf{H}}\mathbf{H}_1^{\mathsf{H}}\mathbf{s}_q + \tilde{w}_{k,q}, \tag{9}$$

where $\mathbf{s}_q = \sum_{k=1}^K \mathbf{f}_{i,q}x_{i,q}$ is the transmit signal vector by the BS, $x_{i,q}$ is the data symbol with $\mathbb{E}\{|x_{i,n}|^2\} = 1$, and $\tilde{w}_{k,q} \sim \mathcal{CN}(0, \sigma^2)$ is complex Gaussian noise at UE k. For the normalization of the precoding vector, we account for the average total power constraint, which is written as

$$\mathbb{E}\{\|\mathbf{s}_q\|^2\} = \mathrm{tr}(\mathbf{F}_q^{\mathsf{H}}\mathbf{F}_q) \leq P_{\max}, \tag{10}$$

where $\mathbf{F}_q = [\mathbf{f}_{1,q}, \ldots, \mathbf{f}_{K,q}] \in \mathbb{C}^{M\times K}$, and $P_{\max} > 0$ denotes the total transmit power.[5] Note that (9) can be written as

$$y_{k,q} = \phi_l^{\mathsf{H}} \mathbf{H}_{k,q}^{\mathsf{H}} \mathbf{f}_{k,q} x_{k,q} + \sum_{i\neq k}^{K} \phi_l^{\mathsf{H}} \mathbf{H}_{k,q}^{\mathsf{H}} \mathbf{f}_{i,q} x_{i,q} + \tilde{w}_{k,q}, \quad (11)$$

while the average received power is

$$\tau_{k,q} = \mathbb{E}\{|y_{k,q}|^2\} = |\phi_l^{\mathsf{H}} \mathbf{H}_{k,q}^{\mathsf{H}} \mathbf{f}_{k,q}|^2 + \sum_{i\neq k}^{K} |\phi_l^{\mathsf{H}} \mathbf{H}_{k,q}^{\mathsf{H}} \mathbf{f}_{i,q}|^2 + \sigma_k^2. \quad (12)$$

The instantaneous SINR at UE k in sector $l, \forall k \in \mathcal{K}, \forall l \in \mathcal{L}$ is written as

$$\gamma_{k,q} = \frac{|\phi_l^{\mathsf{H}} \mathbf{H}_{k,q}^{\mathsf{H}} \mathbf{f}_{k,q}|^2}{\sum_{i\neq k}^{K} |\phi_l^{\mathsf{H}} \mathbf{H}_{k,q}^{\mathsf{H}} \mathbf{f}_{i,q}|^2 + \sigma_k^2}. \quad (13)$$

By assuming Gaussian inputs, the instantaneous rate for UE k at time instance q is given by

$$R_{k,q} = \log_2(1 + \gamma_{k,q}), \quad (14)$$

where $\gamma_{k,q}$ denotes the achievable SINR at time q provided by (13).

Proposition 1: A lower bound of the downlink average SE for UE k of a RIS-aided mMIMO system, which accounts for imperfect CSI and channel aging, is given by

$$\mathrm{SE}_k = \frac{1}{\tau_c} \sum_{q=K+1}^{\tau_c} R_{k,q}, \quad (15)$$

where $\gamma_{k,q}$ is provided by (13).

Proof: Similar to [33], [34], for each q, we compute the achievable SE that includes the achievable SINR $\gamma_{k,q}$, given by (13). Next, we obtain the average over these SEs as in (1). ∎

III. PROBLEM FORMULATION

Herein, we present the formulation of the optimization problem for BD-RIS-assisted MU-MISO systems with imperfect CSI and channel aging, and present methods to jointly design the BD-RIS surface and the transmit precoder.

Given that the BS relies on imperfect instantaneous CSI, we resort to the optimization of the average rate that accounts for the statistical CSI based on a given estimate. In such case, the average rate is given by $\bar{R}_{k,q} = \mathbb{E}_{\mathbf{H}_q|\hat{\mathbf{H}}_q}\{R_{k,q}|\hat{\mathbf{H}}_q\}$, where the ergodic rate at time q is given by the expectation of average rate over $\hat{\mathbf{H}}_q$. Hence, the formulation of the maximization problem is given by

$$(\mathcal{P}1) \quad \max_{\{\mathbf{F}_q\},\{\phi_l \forall l\}} \frac{1}{\tau_c} \sum_{k=1}^{K} \sum_{q=K+1}^{\tau_c} \bar{R}_{k,q} \quad (16a)$$

$$\text{s.t.} \sum_{l,n} |\phi_{l,n}| = 1, \ \forall n, \quad (16b)$$

$$\|\mathbf{F}_q\| \leq P_{\max}, \forall q, \quad (16c)$$

$$\bar{R}_{k,q} \geq R_{k,q}^{\mathrm{th}}, \forall k, \forall q, \quad (16d)$$

where $R_{k,q}^{\mathrm{th}}$ is the threshold rate for UE k that guarantees the QoS. $(\mathcal{P}1)$ is a challenging stochastic optimization problem. To solve $(\mathcal{P}1)$, we are going first to transform it into a deterministic problem by using the SAA method [26], and then apply the WMMSE-rate method [27].[6]

Henceforth, we will rely on the definition below, which provides the SAA of the average rate.

Definition 1: A sample of i.i.d. channels is created from the set $\mathbf{H}_{k,q} = \{\mathbf{H}_{k,q}^{\alpha} = \hat{\mathbf{H}}_{k,q} + \tilde{\mathbf{H}}_{k,q}^{\alpha} | \hat{\mathbf{H}}_{k,q}, \forall \alpha \in \mathcal{A} = \{1, \ldots, A\}\}$, where $\hat{\mathbf{H}}_{k,q}$ is given, while $\tilde{\mathbf{H}}_{k,q}^{\alpha}$ follows the complex Gaussian distribution given as $\mathrm{vec}(\tilde{\mathbf{H}}_{k,q}^{\alpha} \sim \mathcal{CN}(\mathbf{0}, \delta_k^2 \mathbf{I}_{MN})), \forall \alpha \in \mathcal{A}$. In such case, the SAA of the average rate is given by $\hat{R}_{k,q} = \frac{1}{A} \sum_{\alpha} R_{k,q}^{\alpha}, \forall k \in \mathcal{K}$.

We can approximate the stochastic problem $(\mathcal{P}1)$ into the following deterministic problem by taking into account that the SAA of the average rate in Def. 1 is a tight approximation with a large number of samples, which means that $\lim_{A\to\infty} = \hat{R}_{k,q} = \bar{R}_{k,q}$. The deterministic problem is written as

$$(\mathcal{P}2) \quad \max_{\{\mathbf{F}_q\},\{\phi_l \forall l\}} \frac{1}{\tau_c} \sum_{k=1}^{K} \sum_{q=K+1}^{\tau_c} \hat{R}_{k,q} \quad (17a)$$

$$\text{s.t. (16b), (16c),} \quad (17b)$$

$$\hat{R}_{k,q} \geq R_{k,q}^{\mathrm{th}}, \forall k. \quad (17c)$$

The next step, which includes WMMSE-rate reformulation, results in a more tractable form of $(\mathcal{P}2)$. Let $\hat{s}_{k,q}^{\alpha} = g_{k,q}^{\alpha} y_{k,q}^{\alpha}$ be the estimate of $s_{k,q}$ with equalizer $g_{k,q}^{\alpha}$ from UE k in sector $l, \forall k \in \mathcal{K}_l, \forall l \in \mathcal{L}, \forall \alpha \in \mathcal{A}$. Next, we define the MSE function regarding UE k as in sector l at channel sample α as

$$\begin{aligned} e_{k,q}^{\alpha} &= \mathbb{E}\{|\hat{s}_{k,q}^{\alpha} - s_{k,q}^{\alpha}|^2\} \\ &= |g_{k,q}^{\alpha}|^2 \tau_{k,q}^{\alpha} - 2\,\mathrm{Re}\{g_{k,q}^{\alpha} \phi_l^{\mathsf{T}} (\mathbf{H}_{k,q}^{\alpha})^{\mathsf{H}} \mathbf{f}_{k,q}\} + 1. \end{aligned} \quad (18)$$

The optimal unconstrained equalizer that achieves the minimum MSE is obtained as

$$(g_{k,q}^{\alpha})^{\star} = \frac{\mathbf{f}_{k,q}^{\mathsf{H}} \mathbf{H}_{k,q}^{\alpha} \phi_l^*}{\tau_{k,q}^{\alpha}}. \quad (19)$$

The corresponding minimum MSE is given by

$$(e_{k,q}^{\alpha})^{\star} = \min_{g_{k,q}^{\alpha}} e_{k,q}^{\alpha} \quad (20)$$

$$= (1 + \gamma_{k,q}^{\alpha})^{-1}, \forall k \in \mathcal{K}, \forall \alpha \in \mathcal{A}. \quad (21)$$

[5] Since the precoder is applied by the BS and depends on the current CSI that ages, the precoder should depend on the channel use. If we assumed, a fixed precoder, a mismatch would appear between the transmitted signal and the current aged channel.

[6] Although the proposed algorithm is quite fast for jointly optimizing the BD-RIS and the precoding, which means that the algorithm is efficient enough for handling the time-varying channel, we would like to mention that we have not claimed that we provide a solution for a high-mobility scenario, but we just focus on the study of channel aging and its properties.

At time q, the WMMSE-rate relationship is established by introducing the weight $\lambda_{k,q}^{\alpha} \in \mathbb{R}^{+}$ as

$$R_{k,q}^{\alpha} = \max_{\lambda_{k,q}^{\alpha}} \log_2 \lambda_{k,q}^{\alpha} - \lambda_{k,q}^{\alpha}(e_{k,q}^{\alpha})^{\star} + 1, \forall k \in \mathcal{K}, \forall \alpha \in \mathcal{A}. \tag{22}$$

Note that the maximum in (22) is obtained when the weight $\lambda_{k,q}$ satisfies

$$(\lambda_{k,q}^{\alpha})^{\star} = 1 + \gamma_{k,q}^{\alpha}. \tag{23}$$

Hence, $(\mathcal{P}2)$ is reformulated as

$$(\mathcal{P}3) \quad \max_{\substack{\{\lambda_q^{\alpha}, \mathbf{g}_q^{\alpha}, \forall \alpha\} \\ \{\mathbf{F}_q\}, \{\phi_l \forall l\}}} \frac{1}{\tau_c} \sum_{k=1}^{K} \sum_{q=K+1}^{\tau_c} \sum_{\alpha} \frac{1}{A} \left(\log_2 \lambda_{k,q}^{\alpha} - \lambda_{k,q}^{\alpha} e_{k,q}^{\alpha} \right) \tag{24a}$$

$$\text{s.t.} \quad (16b), \ (16c), \tag{24b}$$

$$\frac{1}{A} \sum_{\alpha} \left(\log_2 \lambda_{k,q}^{\alpha} - \lambda_{k,q}^{\alpha}(e_{k,q}^{\alpha}) + 1 \right) \geq R_k^{\text{th}}, \forall k, \tag{24c}$$

where $\boldsymbol{\lambda}_q^{\alpha} = [\lambda_{1,q}^{\alpha}, \ldots, \lambda_{K,q}^{\alpha}]^{\mathsf{T}}$ and $\mathbf{g}_q^{\alpha} = [g_{1,q}^{\alpha}, \ldots, g_{K,q}^{\alpha}]^{\mathsf{T}}, \forall \alpha \in \mathcal{A}$. Problem $(\mathcal{P}3)$ includes a three-block optimization, which although it is not convex, each block with other blocks fixed is convex or more tractable than focusing on the initial objective. In particular, the subproblems with respect to $\{\boldsymbol{\lambda}_q^{\alpha}, \mathbf{g}_q^{\alpha}, \forall \alpha\}$ and $\{\mathbf{F}_q\}$ become convex, while the design of the phase shifts $\{\phi_l, l \in \mathcal{L}\}$ is more tractable. The solution of $\{\boldsymbol{\lambda}_q^{\alpha}, \mathbf{g}_q^{\alpha}, \forall \alpha\}$ with fixed the other two blocks is given in (19), (23). The solutions to blocks $\{\mathbf{F}_q\}$, $\{\phi_l \forall l\}$ follow.

A. SOLUTION TO BLOCK $\{\mathbf{F}_Q\}$

Having fixed the weights, the equalizers, and the BD-RIS matrix, the problem concerning block $\{\mathbf{F}_q\}$ is written as

$$(\mathcal{P}4) \quad \min_{\{\mathbf{F}_q\}} \frac{1}{A} \frac{1}{\tau_c} \sum_{k=1}^{K} \sum_{q=K+1}^{\tau_c} \sum_{\alpha} \lambda_{k,q}^{\alpha} e_{k,q}^{\alpha} \tag{25a}$$

$$\text{s.t.} \quad (16b), \ (24c). \tag{25b}$$

Problem $(\mathcal{P}4)$ can be written as

$$(\mathcal{P}5) \quad \min_{\{\mathbf{f}_{k,q}, \forall k\}} \frac{1}{\tau_c} \sum_{k=1}^{K} \sum_{q=K+1}^{\tau_c} \sum_{k'} \mathbf{f}_{k',q}^{\mathsf{H}} \boldsymbol{\Psi}_{k,q} \mathbf{f}_{k',q} - 2\,\text{Re}\{\boldsymbol{\psi}_{k,q}^{\mathsf{H}} \mathbf{f}_{k,q}\} \tag{26a}$$

$$\text{s.t.} \quad \sum_{k} \|\mathbf{f}_{k,q}\|_2^2 \leq P_{\max}, \tag{26b}$$

$$\sum_{k'} \mathbf{f}_{k',q}^{\mathsf{H}} \boldsymbol{\Psi}_{k,q} \mathbf{f}_{k',q} - 2\,\text{Re}\{\boldsymbol{\psi}_{k,q}^{\mathsf{H}} \mathbf{f}_{k,q}\} \leq \xi_{k,q} - R_{k,q}^{\text{th}}, \forall k, \tag{26c}$$

where we have used the following definitions

$$\boldsymbol{\psi}_{k,q}^{\alpha} = \lambda_{k,q}^{\alpha} g_{k,q}^{\alpha} \mathbf{H}_{k,q}^{\alpha} \phi_l^{*}, \tag{27}$$

$$\boldsymbol{\Psi}_{k,q} = \frac{\boldsymbol{\psi}_{k,q}^{\alpha} (\boldsymbol{\psi}_{k,q}^{\alpha})^{\mathsf{H}}}{\lambda_{k,q}^{\alpha}}, \tag{28}$$

$$\xi_{k,q} = \log_2 \lambda_{k,q}^{\alpha} - \lambda_{k,q}^{\alpha} |g_{k,q}^{\alpha}|^2 \sigma_k^2 - \lambda_{k,q}^{\alpha} + 1, \tag{29}$$

given their averages over A samples, which are $\boldsymbol{\psi}_{k,q} = \frac{1}{A} \sum_{\alpha} \boldsymbol{\psi}_{k,q}^{\alpha}$, $\boldsymbol{\Psi}_{k,q} = \frac{1}{A} \sum_{\alpha} \boldsymbol{\Psi}_{k,q}^{\alpha}$, $\xi_{k,q} = \frac{1}{A} \sum_{\alpha} \xi_{k,q}^{\alpha}, \forall k \in K$.

Problem $(\mathcal{P}5)$ is a convex second-order cone program (SOCP), which can be addressed by interior-point methods having computational complexity $\mathcal{O}((MK+M+K)^{3.5})$ [35].

B. SOLUTION TO BLOCK $\{\boldsymbol{\phi}_L, \forall L\}$

To simplify the design of the block $\{\phi_l, \forall l\}$, the original problem $(\mathcal{P}3)$ can be written without the QoS constraint (24c) as[7]

$$(\mathcal{P}6) \quad \max_{\substack{\{\boldsymbol{\lambda}_q^{\alpha}, \mathbf{g}_q^{\alpha}, \forall \alpha\} \\ \{\mathbf{F}_q\}, \{\phi_l \forall l\}}} \frac{1}{A} \sum_{k} \sum_{q=K+1}^{\tau_c} \sum_{\alpha} \log_2 \lambda_{k,q}^{\alpha} - \lambda_{k,q}^{\alpha} \left(e_{k,q}^{\alpha} \right) \tag{30a}$$

$$\text{s.t.} \quad (16b), \ (16c). \tag{30b}$$

Having fixed the weights, equalizers, and transmit precoder, the problem with respect to the multiple sector BD-RIS becomes

$$(\mathcal{P}7) \quad \min_{\{\phi_l \forall l\}} \sum_{\alpha} \lambda_{k,q}^{\alpha} e_{k,q}^{\alpha} \tag{31a}$$

$$\text{s.t.} \quad \sum_{l} |\phi_{l,n}| = 1, \ \forall n. \tag{31b}$$

Problem $(\mathcal{P}7)$ can be rewritten as

$$(\mathcal{P}8) \quad \min_{\{\phi_l \forall l\}} \left(\phi_l^{\mathsf{H}} \bar{\mathbf{X}}_{l,q} \phi_l - 2\,\text{Re}\{\phi_l^{\mathsf{H}} \bar{\mathbf{x}}_{l,q}\} \right) \tag{32a}$$

$$\text{s.t.} \quad \sum_{l} |\phi_{l,n}| = 1, \ \forall n \tag{32b}$$

where we have used the following definitions

$$\mathbf{v}_{kk',q}^{\alpha} = \mathbf{H}_{k,q}^{\mathsf{T}} \mathbf{f}_{k',q}^{*}, \tag{33}$$

$$X_{k,q}^{\alpha} = \lambda_{k,q}^{\alpha} |g_{k,q}^{\alpha}|^2 \sum_{k'} v_{kk',q}^{\alpha} (v_{kk',q}^{\alpha})^{\mathsf{H}}, \tag{34}$$

$$x_{k,q}^{\alpha} = \lambda_{k,q}^{\alpha} (g_{k,q}^{\alpha})^{*} v_{kk,q}^{\alpha}, \tag{35}$$

$$\bar{X}_{l,q} = \sum_{k' \in \mathcal{K}_l} X_{k',q}, \bar{x}_{l,q} = \sum_{k' \in \mathcal{K}_l} x_{k',q}, \forall l \in \mathcal{L} \tag{36}$$

while the averages over A samples are $X_{k,q} = \frac{1}{A} \sum_{\alpha} X_{k,q}^{\alpha}$, $x_{k,q} = \frac{1}{A} \sum_{\alpha} x_{k,q}^{\alpha}, \forall k \in \mathcal{K}$. The constraints are independent of each other. Hence, we focus on the successive design of each cell while keeping other cells fixed. Below, we provide the design of each cell while others are fixed. In particular, as a first thing, we formulate the problem concerning cell $n, \forall n \in \mathcal{N}$ with other cells fixed as

$$(\mathcal{P}9) \quad \min_{\phi_n} \sum_{l} c_{l,q}(\phi_{l,n}) \tag{37a}$$

[7]The BD-RIS is optimized at each channel use. Otherwise, an optimization at every several channel uses would rely on an outdated cascaded channel $\mathbf{H}_{k,q}$ which changes at each q. In this case, the optimization of the BD-RIS would not correspond to the right channel conditions.

Algorithm 1 A Manifold Solution for Multiple Sector BD-RIS

Input: $\bar{\mathbf{x}}_{l,q}, \bar{\mathbf{X}}_{l,q}, \phi_l, \forall q, \forall l$.
Output:, $\phi_l^\star, \forall l$
Initialize $\phi_l^0 = \phi_l, \forall l \in \mathcal{L}, v = 0$
repeat
  Update $v = v + 1$.
  for $n \in \mathcal{N}$ **do**
  Update $x_{l,j,q}^v$ by (40).
  Update BD-RIS matrix $\{\phi_{n^v}, \forall l\}$ by RCG.
  end for
until convergence

Algorithm 2 Joint Design by Block Coordinate Descent (BCD)

Input: σ_k, $\delta_{k,q}$, $P_{\max}$, $R_{k,q}^{\text{th}}, \forall k, \forall q, \forall l$.
Output: $\mathbf{P}^\star$, $\phi_l^\star, \forall l$.
Initialize ϕ_l^0, $\boldsymbol{\psi}_l^0 = \phi_l^0$, $\mu_l = 0$, $\forall l \in \mathcal{L}$, $\mathbf{F}_q^0$, $v = 0$.
repeat
  Update $v = v + 1$.
  Set weights. $\{\lambda_{k,q}^\alpha, \forall \alpha, \forall q\}^{v-1}$ by (23)
  Set equalizers. $\{\mathbf{g}_{k,q}^\alpha, \forall \alpha, \forall q\}^{v-1}$ by (19)
  Update BD-RIS matrix $\{\phi_{l^v}, \forall l\}$ by Algorithm 1.
  Update precoder $\mathbf{F}_q^v$ by means of SOCP (26).
until convergence

$$\text{s.t.} \quad \|\bar{\phi}_n\|^2 = 1, \tag{37b}$$

where we have

$$c_{l,q}(\phi_{l,n}) = v_{ln,q}|\phi_{l,n}|^2 - 2\,\text{Re}\{\phi_{l,n}^* x_{l,n,q}\} \tag{38}$$

$$v_{l,n,q} = [\bar{X}_{l,q}]_{n,n} \tag{39}$$

$$x_{l,j,q} = \sum_{n \neq j} [\bar{x}_{l,q}]_{j,n} - [\bar{x}_{l,q}]_j \tag{40}$$

$$\bar{\phi}_n = [\phi_{1,n}, \ldots, \phi_{L,n}], \forall n \in \mathcal{N}, \forall l \in \mathcal{K}_l, \forall l \in \mathcal{L} \tag{41}$$

Problem ($\mathcal{P}9$) can be written as

$$(\mathcal{P}10) \quad \bar{\phi}_n^\star = \arg \min_{\|\bar{\phi}_n\|_2^2 = 1} c_q(\bar{\phi}_n), \tag{42a}$$

where $c_q(\bar{\phi}_n) = \sum_l c_{l,q}(\phi_{l,n})$.

Problem ($\mathcal{P}10$) can be addressed by the manifold method because it has a smooth objective function and only one constraint. This optimization can be solved by the Riemannian conjugate gradient (RCG) algorithm [28], which changes the search from Euclidean space to a manifold. The RCG algorithm is described in the Appendix. This approach is used when dealing with optimization problems that have constraints naturally expressed as manifold structures. In Riemannian optimization, the goal is to minimize a smooth function defined on a manifold. The RCG method adapts the principles of the conjugate gradient algorithm by taking into account the geometric structure of the manifold, including the notions of Riemannian gradients and retractions. Algorithm 1 summarizes the solution to each cell of the multiple sector BD-RIS. Its complexity is $\mathcal{O}(I_1 L^{1.5})$, where I_1 is the number of iterations.

An iteration among the above three blocks occurs until convergence by using a block coordinate descent (BCD) algorithm, where each time each block is iteratively optimized while keeping the other blocks fixed. A summary is provided by Algorithm 2.

1) COMPLEXITY ANALYSIS OF THE BCD ALGORITHM

We obtain the complexity of Algorithm 2 by calculating the complexity of the three blocks in steps 6-8. In particular, step 6, i.e., block $\{\lambda_{k,q}^\alpha, \forall \alpha, \forall q\}$ presents complexity $\mathcal{O}(MNKLA)$. The update of block $\mathbf{F}_q$ requires $\mathcal{O}((MK + M + K)^{3.5})$. The update of $\{\phi_{l^v}, \forall l\}$ by Algorithm 1 requires $\mathcal{O}(I_1 L^{1.5})$. Hence, the overall complexity of Algorithm 2 is $\mathcal{O}(I(MK + M + K)^{3.5})$, where I denotes the number of iterations of Algorithm 2 until convergence.[8]

The initialization of Algorithm (2) is as follows. Regarding $\phi_l, \forall l \in \mathcal{L}$, it is initialized as $\phi_l^0 = \frac{1}{\sqrt{L}}[e^{j\varphi_{l,1}}, \ldots, e^{j\varphi_{l,N}}]^{\mathsf{T}}$ with $\varphi_{l,n}$ being randomly selected in $[0, 2\pi], \forall l, \forall n$. In the case of the precoder, it is initialized as $\mathbf{f}_{k,q} = \sum_\alpha \mathbf{H}_{k,q}^\alpha \phi_l^*$ with $\mathbf{f}_{k,q}^0 = \frac{P_{\max}}{K} \frac{\mathbf{f}_{k,q}}{\|\mathbf{f}_{k,q}\|_2}, \forall k$.

IV. NUMERICAL RESULTS

The numerical results of the sum SE for multiple sector BD-RIS-assisted systems with channel aging are presented in this section. Specifically, we first present the simulation layout. Next, we assess the achievable sum SE in terms of certain system parameters, e.g., the severity of channel aging conditions, the number of passive and active antennas, the QoS threshold, and the radiation pattern.

A. SIMULATION SETUP

We consider a single cell having a radius $R = 1000$ meters, where the BS is located in the origin. In particular, the BS is implemented by a uniform linear array having $M = 50$ antennas, which transmit to $K = 15$ mobile UEs. The connection is aided by a multiple sector BD-RIS of $N = 100$ elements. The uplink training duration consists of $\tau = K$ symbols. We assume that the coherence time is $T_c = 2$ ms, and the bandwidth is $B_c = 100$ kHz, i.e., the coherence block consists of 200 channel uses. Moreover, $\sigma^2 = -174 + 10\log_{10} B_c$. For demonstration purposes, the coefficient describing the temporal correlation $\delta_{k,n}$ and the CSI error r_k are assumed the same for all UEs. Furthermore, we assume that the Doppler spread, corresponding is $f_D = 250$ Hz, which corresponds to a relative velocity of 135 km/h between the BS and the UEs. Also, we consider that $T_s = 1/(2W) = 0.025$ μs, describing the symbol time, corresponds to a bandwidth of $W = 20$ MHz.

[8]The overall complexity of the BCD Algorithm is too large and is not suitable for practical BD-RIS. Hence, the topic of future work is to propose algorithms with lower complexity.

TABLE 1. Simulation settings.

Parameters	Value
Transmit/Receive Antenna Gain	$G_{\mathrm{T}} = G_{\mathrm{U}} = 1$
Transmitter-RIS Distance	$d_{\mathrm{T}} = 100$ m
RIS-UE Distance	$d_{\mathrm{U},1} =, \ldots, d_{\mathrm{U},K} = 10$ m
Path Loss Exponent	$\epsilon_{\mathrm{T}} = \epsilon_{\mathrm{U}} = 2.2$
Transmitter-RIS Angle	$\theta_{\mathrm{T}} \in [0, \frac{\pi}{L}]$
RIS-UE Angle	$\theta_{\mathrm{U},k} \in [0, \frac{\pi}{L}], \forall k$
Noise Power	$\sigma_k^2 = -90$ dBm, $\forall k$
CSI Error	$r_k^2 = 0.1, \forall k$
Number of Samples	$A = 50$
Number of Sectors	$L = 5$
Number of UEs per Sector	$K_l = 3$
Number of BD-RIS antennas per Sector	$N = N_{\mathrm{h}} \times N_{\mathrm{v}} = 5 \times 6 = 30$
Number of transmit antennas	$M = 5$
QoS Threshold per UE	$R_{k,q}^{\mathrm{th}} = R^{\mathrm{th}} = 0.2, \forall k, \forall q$

We have the following path loss model [16][9]

$$\beta_k = \begin{cases} \rho(1 - \cos\frac{\pi}{L})^2 & \text{Idealized pattern,} \\ \frac{\rho}{(a_L+1)^2(\cos\theta_{\mathrm{T}}\cos\theta_{\mathrm{U},k})^{a_L}} & \text{Practical pattern,} \end{cases} \quad (43)$$

where $\rho = \frac{4^3\pi^4 d_{\mathrm{T}}^{\epsilon_{\mathrm{T}}} d_{\mathrm{U},k}^{\epsilon_{\mathrm{U}}}}{\lambda^4 G_{\mathrm{T}} G_{\mathrm{U}}}$ with d_{T} being the distance between the transmitter (BS) and the BD-RIS, $d_{\mathrm{U},k}$ being the distance between the BD-RIS and UE k, ϵ_{T} and ϵ_{U} being the corresponding path loss exponents, λ being the wavelength of the transmit signal, G_{T} and G_{U} being the transmit and receive antenna gains. Also, a_L is a parameter concerning the beamwidth of the BD-RIS antennas, θ_{T} denotes the elevation angle between the transmit and BD-RIS antennas, and $\theta_{\mathrm{U},k}$ denotes the elevation angle from the BD-RIS antenna to UE k. Each sector of the multiple sector BD-RIS is designed as a uniform planar array (UPA) with $N_{\mathrm{h}} \times N_{\mathrm{v}} = N$ elements, where N_{h} and N_{v} are the numbers elements in the horizontal and vertical direction, respectively. Moreover, UEs in the l sector are uniformly located. Monte Carlo (MC) simulations provide the ergodic sum rate for 10^3 independent channel realizations. Table 1 provides the simulation settings.

Fig. 2 depicts the effect of channel aging in terms of the achievable sum SE with respect to the number of BS antennas M for different velocities. The sum rate increases with M. Also, we observe a decrease in the sum rate with an increase in the velocity. For comparison, we have provided the solid red line with the help of MC simulation that corresponds to the conventional RIS [25] when $v = 10$ km/h. Clearly, the BD-RIS outperforms the conventional RIS setting.

Fig. 3 depicts the achievable sum SE against the number of RIS elements N for different v. The achievable sum SE increases with N. However, the performance is degraded as the velocity increases. As the velocity increases, the loss in the sum SE becomes larger. Notably, the degradation due to mobility can be compensated with an increment regarding the number of BD-RIS elements. Also, we have plotted the performance of STAR-RIS and conventional RIS. Obviously, the multiple sector BD-RIS performs better even in channel aging conditions due to its highly directional beam at each sector.

In Fig. 4, we depict the achievable sum SE with respect to the transmit power for varying relative velocity v. By increasing the transmit power, the achievable sum SE increases. For a given transmit power, the performance worsens as the mobility of UES increases. To counterbalance this worsening, an increase in the transmit power is another solution.

In Fig. 5, we show the achievable sum SE versus the QoS threshold for different relative velocities v and radiation patterns (idealized and practical). It is shown that the achievable ergodic sum SE decreases with the growth of the QoS threshold. Moreover, the idealized pattern scheme performs always better compared to the practical pattern scheme.

In Fig. 6, we show the achievable sum SE against the number of iterations for different radiation patterns and relative velocities v. Specifically, as we increase the velocity the overall algorithm converges at a larger number of iterations.

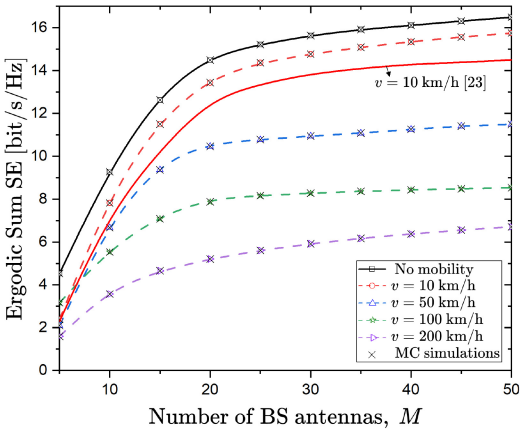

FIGURE 2. Achievable sum SE against the number of BS antennas M for varying velocity v (Analytical results and MC simulations).

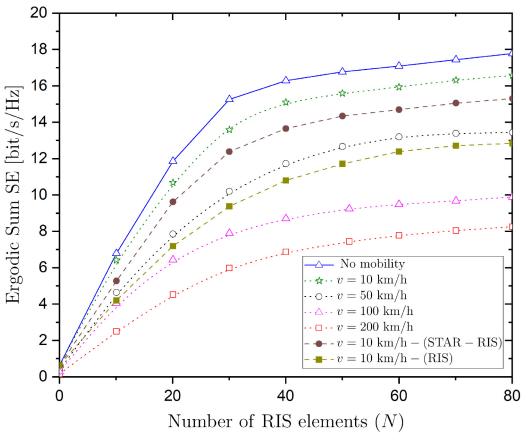

FIGURE 3. Achievable sum SE against the number of RIS elements N for varying velocity v.

[9]The idealized pattern is obtained by assuming a 100% radiation efficiency based on antenna theory for each antenna of the L-sector BD-RIS. More details on the derivations of the idealized and practical patterns can be found on [12].

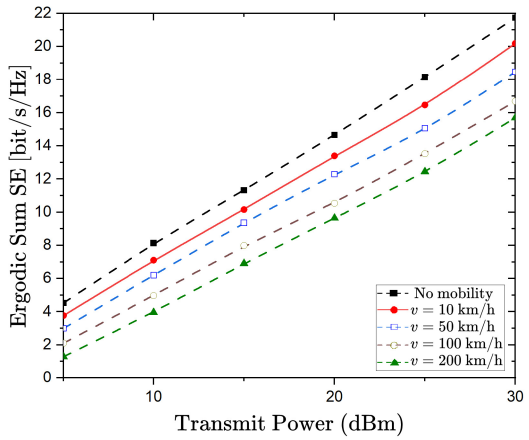

FIGURE 4. Achievable sum SE against the transmit power for varying velocity v.

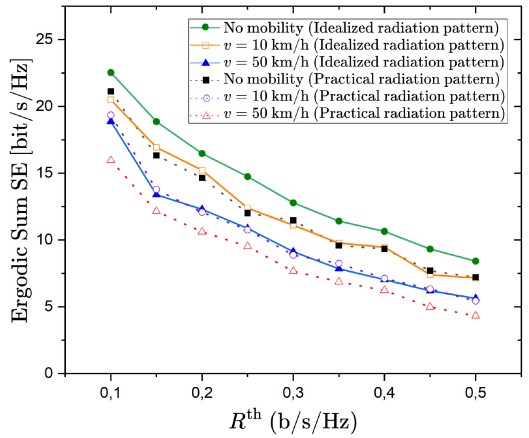

FIGURE 5. Achievable sum SE against the transmit power for different velocities v and radiation patterns.

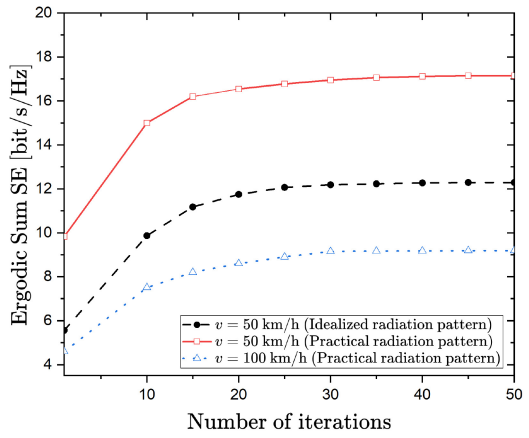

FIGURE 6. Achievable sum SE against the number of iterations for different radiation patterns and velocities v.

A similar observation is made with respect to the radiation pattern. In particular, the practical radiation pattern requires a larger number of iterations for the algorithm to converge.

In Fig. 7, we illustrate the achievable sum SE against the number of elements N for different numbers of samples A. A larger number of samples will improve the performance,

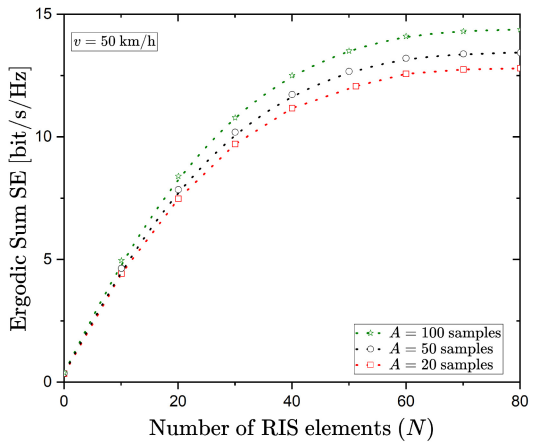

FIGURE 7. Achievable sum SE against the number of RIS elements N for varying number of samples A.

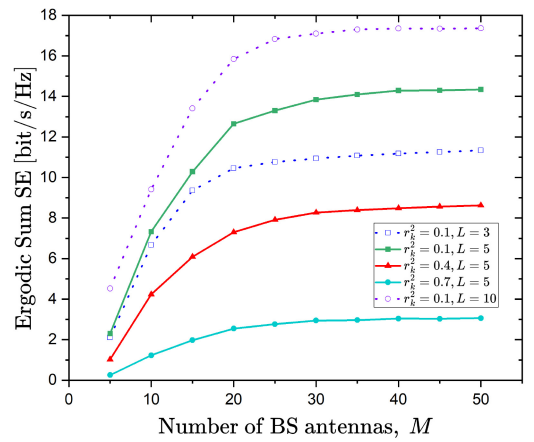

FIGURE 8. Achievable sum SE against the number of BS antennas M for varying CSI error r_k^2 and number of sectors L.

but will also increase the computational cost. However, there is a trade-off between performance and computational cost for the selection of the number of samples A. This can be decided by performing several trials.

Fig. 8 depicts the impact of the CSI error r_k^2 (solid lines) and number of sectors L (dotted lines) in terms of the achievable sum SE with respect to the number of BS antennas M. First, we increase the CSI error r_k^2 from 0.1 to 0.7, and we observe that performance worsens as expected. In the case of an increase to the number of sectors L from 3 to 10, the rate increases since by increasing L, the beamwidth of each BD-RIS antenna, i.e., the antenna gain of each BD-RIS antenna increases.

V. CONCLUSION

We considered the effect of channel aging on multiple sector BD-RIS in a MU-MISO communications system. We jointly optimized the multiple sectors BD-RIS and the transmit precoder by using the SAA and the WMMSE-rate relationship to transform the stochastic optimization problem regarding the maximisation of the average sum SE into a more tractable deterministic problem. In the case

of the BD-RIS matrix, we applied the RCG algorithm. Finally, numerical results demonstrated the effect of channel aging and its relationship with other system parameters. For example, an increase in the amount of the number of BD-RIS elements can compensate for the degradation due to challenge aging. A future research direction is the study of channel aging on BD-RIS-assisted systems by using statistical CSI. This method achieves an overhead reduction since the optimization takes place every several coherence intervals, and its complexity is low [4], [25], [30]. Another possible extension of this work is to apply a Wiener predictor to mitigate channel aging [21].

APPENDIX
THE RCG ALGORITHM

The RCG algorithm relies on the fact that it is the modified version of the CG. Hence, the Riemannian gradient in RCG can be derived from the Euclidean gradient. Specifically, the gradient of the function

$$c_q\big(\bar{\phi}_n\big) = \sum_l c_{l,q}(\bar{\phi}_{l,n}) \tag{44}$$

is given by

$$\nabla c_q\big(\bar{\phi}_n\big) = \left[\frac{\partial c_q\big(\bar{\phi}_n\big)}{\partial \phi_{1,n}}, \ldots, \frac{\partial c_q\big(\bar{\phi}_n\big)}{\partial \phi_{l,n}}\right], \tag{45}$$

$$= [\nabla c_{1,q}(\phi_{1,n}), \ldots, \nabla c_{L,q}(\phi_{L,n})], \tag{46}$$

where

$$\nabla c_{l,q}(\bar{\phi}_{l,n}) = 2v_{l,n,q}\phi_{l,n} - 2x_{l,n,q}. \tag{47}$$

The next step includes the derivation of the Riemannian gradient, which results from the projection of the Euclidean gradient onto the tangent space. In other words, we have

$$\nabla_{\mathbb{N}} c_q\big(\bar{\phi}_n\big) = \mathrm{Pr}_{\bar{\phi}_n}\big(\nabla c_q\big(\bar{\phi}_n\big)\big) \tag{48}$$

$$= \nabla c_q\big(\bar{\phi}_n\big) - \mathrm{Re}\big\{\mathrm{tr}\big(\bar{\phi}_n^{\mathrm{H}} \nabla c_q\big(\bar{\phi}_n\big)\phi_n\big)\bar{\phi}_n\big\}. \tag{49}$$

Thus, the direction at the ith iteration is given by

$$\boldsymbol{\beta}^i = -\nabla_{\mathbb{N}} c_q\Big(\bar{\phi}_n^i\Big) + \mu^i \mathrm{Pr}\bar{\phi}_n(\boldsymbol{\beta}^{i-1}), \tag{50}$$

where μ^i corresponds to the Riemannian version of the Polak-Ribière expression [28], provided by

$$\mu^i = \frac{\Big\langle \nabla_{\mathbb{N}} c_q\big(\bar{\phi}_n^i\big), \nabla_{\mathbb{N}} c_q\big(\bar{\phi}_n^i\big) - \mathrm{Pr}_{\bar{\phi}_n^i}\big(\nabla_{\mathbb{N}} c_q\big(\bar{\phi}_n^{i-1}\big)\Big\rangle}{\Big\langle \nabla_{\mathbb{N}} c_q\Big(\bar{\phi}_n^{i-1}\Big), \nabla_{\mathbb{N}} c_q\Big(\bar{\phi}_n^{i-1}\Big)\Big\rangle}, \tag{51}$$

where $\langle A, B\rangle = \mathrm{Re}\{\mathrm{tr}(\mathbf{A}^{\mathrm{H}}\mathbf{B})\}$. The $i+1$th iteration is provided by [28]

$$\bar{\phi}_n^{i+1} = \frac{\bar{\phi}_n^i + u^i \boldsymbol{\beta}^i}{\|\bar{\phi}_n^i + u^i \boldsymbol{\beta}^i\|_2}, \tag{52}$$

where u^i denotes the step size provided by Armijo backtracking [28]. The procedure, updating iteratively the stepsize, the retraction, the Polak-Ribière formula, and the search direction, continues until convergence.

REFERENCES

[1] E. Basar, M. Di Renzo, J. De Rosny, M. Debbah, M.-S. Alouini, and R. Zhang, "Wireless communications through reconfigurable intelligent surfaces," *IEEE Access*, vol. 7, pp. 116753–116773, 2019.

[2] Q. Wu and R. Zhang, "Intelligent reflecting surface enhanced wireless network via joint active and passive beamforming," *IEEE Trans. Wireless Commun.*, vol. 18, no. 11, pp. 5394–5409, Nov. 2019.

[3] C. Pan et al., "Multicell MIMO communications relying on intelligent reflecting surfaces," *IEEE Trans. Wireless Commun.*, vol. 19, no. 8, pp. 5218–5233, Aug. 2020.

[4] A. Papazafeiropoulos, C. Pan, P. Kourtessis, S. Chatzinotas, and J. M. Senior, "Intelligent reflecting surface-assisted MU-MISO systems with imperfect hardware: Channel estimation, beamforming design," *IEEE Trans. Wireless Commun.*, vol. 21, no. 3, pp. 2077–2092, Mar. 2022.

[5] J. Xu, Y. Liu, X. Mu, and O. A. Dobre, "STAR-RISs: Simultaneous transmitting and reflecting reconfigurable intelligent surfaces," *IEEE Commun. Lett.*, vol. 25, no. 9, pp. 3134–3138, Sep. 2021.

[6] X. Mu, Y. Liu, L. Guo, J. Lin, and R. Schober, "Simultaneously transmitting and reflecting (STAR) RIS aided wireless communications," *IEEE Trans. Wireless Commun.*, vol. 21, no. 5, pp. 3083–3098, May 2022.

[7] S. Shen, B. Clerckx, and R. Murch, "Modeling and architecture design of reconfigurable intelligent surfaces using scattering parameter network analysis," *IEEE Trans. Wireless Commun.*, vol. 21, no. 2, pp. 1229–1243, Feb. 2022.

[8] Q. Li et al., "Reconfigurable intelligent surfaces relying on non-diagonal phase shift matrices," *IEEE Trans. Veh. Technol.*, vol. 71, no. 6, pp. 6367–6383, Jun. 2022.

[9] H. Li, S. Shen, and B. Clerckx, "Beyond diagonal reconfigurable intelligent surfaces: From transmitting and reflecting modes to single-, group-, and fully-connected architectures," *IEEE Trans. Wireless Commun.*, vol. 22, no. 4, pp. 2311–2324, Apr. 2023.

[10] M. Nerini, S. Shen, and B. Clerckx, "Optimal group and fully connected design for beyond diagonal reconfigurable intelligent surfaces," 2022, *arXiv:2211.06117*.

[11] M. Nerini, S. Shen, and B. Clerckx, "Discrete-value group and fully connected architectures for beyond diagonal reconfigurable intelligent surfaces," 2021, *arXiv:2110.00077*.

[12] H. Li, S. Shen, and B. Clerckx, "Beyond diagonal reconfigurable intelligent surfaces: A multi-sector mode enabling highly directional full-space wireless coverage," *IEEE J. Sel. Areas Commun.*, vol. 41, no. 8, pp. 2446–2460, Aug. 2023.

[13] Y. Dong, Q. Li, S. X. Ng, and M. El-Hajjar, "Reconfigurable intelligent surface relying on low-complexity joint sector non-diagonal structure," *IEEE Open J. Veh. Technol.*, vol. 5, pp. 1106–1123, Aug. 2024.

[14] Q. Li, M. El-Hajjar, I. Hemadeh, A. Shojaeifard, and L. Hanzo, "Coordinated reconfigurable intelligent surfaces: Non-diagonal group-connected design," *IEEE Trans. Veh. Tech.*, vol. 73, no. 7, pp. 10811–10816, Jul. 2024.

[15] H. Zhang et al., "Intelligent omni-surfaces for full-dimensional wireless communications: Principles, technology, and implementation," *IEEE Commun. Mag.*, vol. 60, no. 2, pp. 39–45, Feb. 2022.

[16] H. Li, S. Shen, and B. Clerckx, "Synergizing beyond diagonal reconfigurable intelligent surface and rate-splitting multiple access," 2023, *arXiv:2303.06912*.

[17] D. Mishra and H. Johansson, "Channel estimation and low-complexity beamforming design for passive intelligent surface assisted MISO wireless energy transfer," in *Proc. Int. Conf. Acoust., Speech Signal Process. (ICASSP)*, 2019, pp. 4659–4663.

[18] Z.-Q. He and X. Yuan, "Cascaded channel estimation for large intelligent metasurface assisted massive MIMO," *IEEE Wireless Commun. Lett.*, vol. 9, no. 2, pp. 210–214, Feb. 2020.

[19] A. M. Elbir, A. Papazafeiropoulos, P. Kourtessis, and S. Chatzinotas "Deep channel learning for large intelligent surfaces aided mm-Wave massive MIMO systems," *IEEE Wireless Commun. Lett.*, vol. 9, no. 9, pp. 1447–1451, Sep. 2020.

[20] K. Truong and R. Heath, "Effects of channel aging in massive MIMO systems," *J. Commun. Netw.*, vol. 15, no. 4, pp. 338–351, Aug. 2013.

[21] A. K. Papazafeiropoulos and T. Ratnarajah, "Deterministic equivalent performance analysis of time-varying massive MIMO systems," *IEEE Trans. Wireless Commun.*, vol. 14, no. 10, pp. 5795–5809, Oct. 2015.

[22] A. K. Papazafeiropoulos, "Impact of general channel aging conditions on the downlink performance of massive MIMO," *IEEE Trans. Veh. Technol.*, vol. 66, no. 2, pp. 1428–1442, Feb. 2017.
[23] R. Chopra et al., "Performance analysis of FDD massive MIMO systems under channel aging," *IEEE Trans. Wireless Commun.*, vol. 17, no. 2, pp. 1094–1108, Feb. 2018.
[24] Y. Chen, Y. Wang, and L. Jiao, "Robust transmission for reconfigurable intelligent surface aided millimeter wave vehicular communications with statistical CSI," *IEEE Trans. Wireless Commun.*, vol. 21, no. 2, pp. 928–944, Feb. 2022.
[25] A. Papazafeiropoulos, I. Krikidis, and P. Kourtessis, "Impact of channel aging on reconfigurable intelligent surface aided massive MIMO systems with statistical CSI," *IEEE Trans. Veh. Tech.*, vol. 72, no. 1, pp. 689–703, Jan. 2023.
[26] A. Shapiro, D. Dentcheva, and A. Ruszczynski, *Lectures on Stochastic Programming: Modeling and Theory*. Philadelphia, PA, USA: SIAM, 2021.
[27] S. S. Christensen, R. Agarwal, E. De Carvalho, and J. M. Cioffi, "Weighted sum-rate maximization using weighted MMSE for MIMO-BC beamforming design," *IEEE Trans. Wireless Commun.*, vol. 7, no. 12, pp. 4792–4799, Dec. 2008.
[28] N. Boumal, "Optimization and estimation on manifolds," Ph.D. dissertation, Dept. Electron. Appl. Math., Inst. Inf. Commun. Technol., Žilina, Slovenské, 2014.
[29] C. You, B. Zheng, W. Mei, and R. Zhang, "How to deploy intelligent reflecting surfaces in wireless network: BS-side, user-side, or both sides?" *J. Commun. Inf. Net.*, vol. 7, no. 1, pp. 1–10, 2022.
[30] A. Kammoun et al., "Asymptotic max-min SINR analysis of reconfigurable intelligent surface assisted MISO systems," *IEEE Trans. Wireless Commun.*, vol. 19, no. 12, pp. 7748–7764, Dec. 2020.
[31] Q.-U.-A. Nadeem, H. Alwazani, A. Kammoun, A. Chaaban, M. Debbah, and M.-S. Alouini, "Intelligent reflecting surface-assisted multi-user MISO Communication: Channel estimation and beamforming design," *IEEE Open J. Commun. Soc.*, vol. 1, pp. 661–680, 2020.
[32] S. M. Kay, *Fundamentals of Statistical Signal Processing: Estimation Theory*. Upper Saddle River, NJ, USA: Prentice-Hall, 1993.
[33] E. Björnson, M. Matthaiou, and M. Debbah, "Massive MIMO with non-ideal arbitrary arrays: Hardware scaling laws and circuit-aware design," *IEEE Trans. Wireless Commun.*, vol. 14, no. 8, pp. 4353–4368, Aug. 2015.
[34] A. Pitarokoilis, S. Mohammed, and E. Larsson, "Uplink performance of time-reversal MRC in massive MIMO systems subject to phase noise," *IEEE Trans. Wireless Commun.*, vol. 14, no. 2, pp. 711–723, Feb. 2015.
[35] S. Boyd, S. P. Boyd, and L. Vandenberghe, *Convex Optimization*. Cambridge, MA, USA: MIT Press, 2004.

ANASTASIOS PAPAZAFEIROPOULOS (Senior Member, IEEE) received the B.Sc. degree (Hons.) in physics, the M.Sc. degree (Hons.) in electronics and computers science, and the Ph.D. degree from the University of Patras, Greece, in 2003, 2005, and 2010, respectively. From 2011 to 2012 and from 2016 to 2017, he was with the Institute for Digital Communications, University of Edinburgh, U.K., as a Postdoctoral Research Fellow. From 2012 to 2014, he was a Research Fellow with Imperial College London, U.K., awarded with a Marie Curie fellowship (IEF-IAWICOM). He is currently a Vice-Chancellor Fellow with the University of Hertfordshire, U.K. He is also a Visiting Research Fellow with the SnT, University of Luxembourg, Luxembourg. He has been involved in several EPSRC and EU FP7 Projects, such as HIATUS and HARP. His research interests span machine learning for wireless communications, intelligent reflecting surfaces, massive MIMO, heterogeneous networks, 5G and beyond wireless networks, full-duplex radio, mm-wave communications, random matrix theory, hardware-constrained communications, and performance analysis of fading channels. In addition, he has been listed as the Worlds Top 2% Scientist by Stanford University since 2019. He is currently serving as an Editor for the IEEE COMMUNICATIONS LETTERS, where he has been also recognized as an Exemplary Editor.

PANDELIS KOURTESSIS is the Director of the Centre for Engineering Research and a Reader of Communication Networks with the University of Hertfordshire, U.K., leading the activities of the Networks Engineering Research Group into Communications and Information Engineering, including next generation passive optical networks, optical and wireless MAC protocols, 5G RANs, software defined network and network virtualization 5G and satellite networks, and more recently machine learning for next generation networks. His funding ID includes EU COST, FP7, H2020, European Space Agency, UKRI, and industrially funded projects. He has served as the general chair, the co-chair, and a technical programme committee member, and at the scientific committees and expert groups of IEEE workshops and conferences, European Technology Platforms and European Networks of Excellence. He has published more than 80 papers at peer-reviewed journals, peer-reviewed conference proceedings, and international conferences. His research has received coverage at scientific journals, magazines, white papers, and international workshops. He has been a co-editor of a Springer book and a Chapter Editor of an IET book on softwarization for 5G.

SYMEON CHATZINOTAS (Fellow, IEEE) is currently a Full Professor/Chief Scientist I and the Head of the SIGCOM Research Group, SnT, University of Luxembourg. In the past, he was a Visiting Professor with the University of Parma, Italy, lecturing on "5G Wireless Networks." He is coordinating the research activities on communications and networking, acting as a PI for more than 20 projects and main representative for 3GPP, ETSI, and DVB. He has (co-)authored more than 450 technical papers in refereed international journals, conferences and scientific books. He was involved in numerous research and development projects for NCSR Demokritos, CERTH Hellas and CCSR, University of Surrey. He was the co-recipient of the 2014 IEEE Distinguished Contributions to Satellite Communications Award and the Best Paper Awards at EURASIP JWCN, CROWNCOM, and ICSSC. He is currently in the editorial board of the IEEE TRANSACTIONS ON COMMUNICATIONS, IEEE OPEN JOURNAL OF VEHICULAR TECHNOLOGY, and the *International Journal of Satellite Communications and Networking*.